ISSN 1674-1056
http://cpb.iphy.ac.cn
http://iopscience.iop.org/cpb
中国物理 B
Chinese Physics
中国物理 Chinese Physics B

Isostructural phase transition-induced bulk modulus multiplication in dopant stabilized ZrO_2 solid solution

Min Wang(王敏), Wen-Shu Shen(沈文舒), Xiao-Dong Li(李晓东), Yan-Chun Li(李延春), Guo-Zhao Zhang(张国召), Cai-Long Liu(刘才龙), Lin Zhao(赵琳), Shu-Peng Lv(吕舒鹏), Chun-Xiao Gao(高春晓), Yong-Hao Han(韩永昊)
Citation: Chin. Phys. B . 2019, 28(7): 076109. **doi:** 10.1088/1674-1056/28/7/076109
Journal homepage: http://cpb.iphy.ac.cn; http://iopscience.iop.org/cpb

What follows is a list of articles you may be interested in

Quantum density functional theory studies of structural, elastic, and opto-electronic properties of $ZMoO_3$(Z=Ba and Sr) under pressure

Saad Tariq, A A Mubarak, Saher Saad, M Imran Jamil, S M Sohail Gilani
Chin. Phys. B . 2019, 28(6): 066101. **doi:** 10.1088/1674-1056/28/6/066101

Crystal structures and decomposing of B-P compounds under pressure

Die Zhang(张蝶), Xilian Jin(靳锡联), Quan Zhuang(庄全), Ying Li(李颖), Shuhan Yang(杨淑涵), Liying Song(宋丽莹), Bingbing Liu(刘冰冰), Tian Cui(崔田)
Chin. Phys. B . 2019, 28(5): 056101. **doi:** 10.1088/1674-1056/28/5/056101

Function of large-volume high-pressure apparatus at SECUF

Pinwen Zhu(朱品文), Qiang Tao(陶强), Lu Wang(王璐), Zhi He(何志), Tian Cui(崔田)
Chin. Phys. B . 2018, 27(7): 076103. **doi:** 10.1088/1674-1056/27/7/076103

Polycrystalline cubic boron nitride prepared with cubic-hexagonal boron nitride under high pressure and high temperature

Ming Yang(杨鸣), Zi-Li Kou(寇自力), Teng Liu(刘腾), Jing-Rui Lu(卢景瑞), Fang-Ming Liu(刘方明), Yin-Juan Liu(刘银娟), Lei Qi(戚磊), Wei Ding(丁未), Hong-Xia Gong(龚红霞), Xiao-Lin Ni(倪小林), Duan-Wei He(贺端威)
Chin. Phys. B . 2018, 27(5): 056105. **doi:** 10.1088/1674-1056/27/5/056105

Compression behavior and phase transition of β-Si_3N_4 under high pressure

Hong-xia Gong(龚红霞), Zi-li Kou(寇自力), Cong Fan(樊聪), Hao Liang(梁浩), Qi-ming Wang(王齐明), Lei-lei Zhang(张雷雷), Fang Peng(彭放), Ming Yang(杨鸣), Xiao-lin Ni(倪小林), Jing Liu(刘景)
Chin. Phys. B . 2018, 27(5): 056101. **doi:** 10.1088/1674-1056/27/5/056101

Isostructural phase transition-induced bulk modulus multiplication in dopant-stabilized ZrO_2 solid solution*

Min Wang(王敏)[1], Wen-Shu Shen(沈文舒)[1], Xiao-Dong Li(李晓东)[2], Yan-Chun Li(李延春)[2], Guo-Zhao Zhang(张国召)[1], Cai-Long Liu(刘才龙)[1], Lin Zhao(赵琳)[1], Shu-Peng Lv(吕舒鹏)[1], Chun-Xiao Gao(高春晓)[1], and Yong-Hao Han(韩永昊)[1,†]

[1] *State Key Laboratory of Superhard Materials, Jilin University, Changchun* 130012, *China*

[2] *Beijing Synchrotron Radiation Facility, Institute of High Energy Physics, Chinese Academy of Sciences, Beijing* 100049, *China*

(Received 31 January 2019; revised manuscript received 14 May 2019; published online 11 June 2019)

The electrical transport properties and structures of Y_2O_3/ZrO_2 solid solution have been studied under high pressure up to 23.2 GPa by means of *in situ* impedance spectroscopy and x-ray diffraction (XRD) measurements. In the impedance spectra, it can be found that the pressure-dependent resistance of Y_2O_3/ZrO_2 presents two different change trends before and after 13.3 GPa, but the crystal symmetry still remains stable in the cubic structure revealed by the XRD measurement and Rietveld refinement. The pressure dependence of the lattice constant and unit cell volume shows that the Y_2O_3/ZrO_2 solid solution undergoes an isostructural phase transition at 13.1 GPa, which is responsible for the abnormal change in resistance. By fitting the volume data with the Birch–Murnaghan equation of state, we found that the bulk modulus B_0 of the Y_2O_3/ZrO_2 solid solution increases by 131.9% from 125.2 GPa to 290.3 GPa due to the pressure-induced isostructural phase transition.

Keywords: high pressure, x-ray diffraction, crystal structure, Y_2O_3/ZrO_2

PACS: 61.05.cp, 61.50.–f, 91.60.Gf **DOI:** 10.1088/1674-1056/28/7/076109

1. Introduction

Zirconia (ZrO_2) is involved in many applications, such as foundry ceramics, refractories, paint pigments, fuel cells, and solid electrolytes in oxygen sensors, due to its outstanding chemical and physical properties including high hardness, high thermal conductivity, and high ionic conductivity.[1–3] ZrO_2 has abundant phases at high temperatures: the monoclinic phase can be thermodynamically stable from room temperature to about 1100 ℃, and then crystallize into a tetragonal phase at 1100 ℃ and a cubic phase at 1900 ℃.[4–6] To quench these high-temperature tetragonal and cubic phases to ambient conditions, cations with a valence lower than 4^+, such as Y^{3+}, La^{3+}, Mg^{2+}, and Ca^{2+} are doped, by which CeO_2/ZrO_2, CaO/ZrO_2, MgO/ZrO_2, and Y_2O_3/ZrO_2 (cubic) solid solutions are formed.

Important technical applications can be found in dopants. For example, transient optical measurements of materials under impact compression usually require different types of optical windows.[7–9] Dolan *et al.*[8] reported a new optical window material based on dopant-stabilized cubic ZrO_2). At present, doping Y_2O_3 to obtain cubic ZrO_2) is a common method.[10] A low impact pressure experimental study showed that cubic ZrO_2) can be used as an optical window material and is a preferred substitute for sapphire window materials.[8]

Recently, there has been growing interest in the connection between the electrical properties and microstructures of dopant-stabilized ZrO_2.[11–14] It is found that Sc_2O_3-stabilized ZrO_2 solid solution with the cubic fluorite structure shows the highest conductivity among all ZrO_2)-based electrolytes.[15,16] This provides potential to lower the operating temperature of the ZrO_2)-based electrochemical devices, and makes the synthesis of the cubic structure ZrO_2 an attractive goal. With the co-precipitate method, Y_2O_3-stabilized ZrO_2 powders in the cubic structure have been directly synthesized, and the particle size is uniform.[17,18]

As another state parameter that is independent of temperature and chemical composition, pressure tunes the physical properties of materials by compressing the distance between atoms and modifying the electronic structures.[19,20] The phase transitions of ZrO_2 under high pressure have been studied systematically with various techniques. It undergoes the phase transition sequence of baddeleyite (MI, monoclinic, space group: $P2_1/c$) $\rightarrow$ orthorhombic I (OI, orthorhombic, space group: *Pbca*) at 11.8 GPa $\rightarrow$ orthorhombic II (OII, orthorhombic, space group: *Pnma*) at 26.2 GPa.[21,22] However, similar studies on dopant-stabilized ZrO_2 solid solutions under high pressures are still lacking. Inspired by the aforementioned issues, we synthesize the Y_2O_3-stabilized ZrO_2 solid solution, and study its electrical transport and structural properties *in situ* at high pressures. An abnormal change is found in the electrical transport properties, and its physical origin, a pressure-induced isostructural phase transition, is revealed.

*Project supported by the National Key Research and Development Program of China (Grant No. 2018YFA0305900) and the National Natural Science Foundation of China (Grant Nos. 11774126, 11774174, 1674404, and 51772125).

†Corresponding author. E-mail: hanyh@jlu.edu.cn

© 2019 Chinese Physical Society and IOP Publishing Ltd

2. Experimental methods

ZrO_2/Y_2O_3 samples were prepared by the co-precipitate method. First, a weight of 2.58 g of zirconyl chloride ($ZrOCl_2{\cdot}8\ H_2O$) was dissolved in deionized water. Next, 1.56 g YCl_3 was dissolved into the solution to form the Y_2O_3-doped ZrO_2), and then NH_4OH was gradually added to the solution until the pH value was equal to 10. The solution was continuously stirred throughout the process. After reaction, the final product was repeatedly filtered and washed by deionized water to remove the chlorine ions (NH_4Cl), residual NH_3, and other anionic impurities; the product was subsequently settled by centrifugal separation of 10000 rpm for 10 min until the supernatants became clear. After drying at 100 ℃ for 2 h, the final samples were calcined at 800 ℃ for 2 h with a heating rate of 5 ℃·min^{-1} in a muffle furnace under air atmosphere.

In order to identify the constitution and chemical valences, the samples were further analyzed by x-ray photoelectron spectroscopy (XPS). XPS was done on a PerkinElmer PHI 5000CESCA system to analyze the electronic states. All the binding energies were calibrated via the contaminant carbon (C 1s = 284.6 eV) as a reference. The initial structure of the sample was confirmed by x-ray diffraction (XRD) measurements.

High-pressure experiments were conducted in a diamond anvil cell with the anvil culet with a diameter of 300 μm.[23] A piece of T301 stainless steel was pre-indented to a thickness of 60 μm, and then drilled by a laser to make a hole 150 μm in diameter at the center of the indentation. A mixture of cubic boron nitride powders and epoxy was compressed into the indentation as the insulating layer. Subsequently, another hole (diameter of 100 μm) was drilled and served as a sample chamber. The impedance spectra were measured with parallel plate electrodes. The fabrication process of the electrodes on two diamond anvils has been reported in previous studies.[24–26] Pressure was calibrated by the shift of the ruby fluorescent R1 line.[27] No pressure medium was loaded into the sample in order to avoid introducing impurities for the electrical measurement and also to ensure a good electrical contact between the sample and electrodes.

The impedance spectra were measured by a Solartron 1260 impedance analyzer equipped with a Solartron 1296 dielectric interface. An alternate-current sine signal with an amplitude of 1 V was sent to the sample, and its frequency ranged from 0.1 Hz to 10^7 Hz. For electrical measurements, the pressure was loaded up to 23.2 GPa.

The *in situ* high-pressure angle-dispersive XRD measurements were conducted at beamline 4W2 of the Beijing Synchrotron Radiation Facility.[28] The x-ray wavelength is 0.6199 Å. For better comparison with the measurements of the electrical transport properties, no pressure-transmitting medium was loaded. The distance between the sample and the detector, and the parameters of the detector, were calibrated with the CeO_2 standard. Bragg's diffraction images were integrated using Fit2d software, yielding one-dimensional intensity versus diffraction angle 2θ patterns. The Rietveld refinements of crystal structures were performed using the program Materials Studio.

3. Results and discussion

The XPS spectra (Figs. 1(a)–1(d)) reveal that the sample is composed of O, Y, and Zr elements. The C 1s peak comes from the adventitious carbon contamination in the XPS instrument. The specific high-resolution XPS spectra of the elements are shown in Figs. 1(a)–1(c).

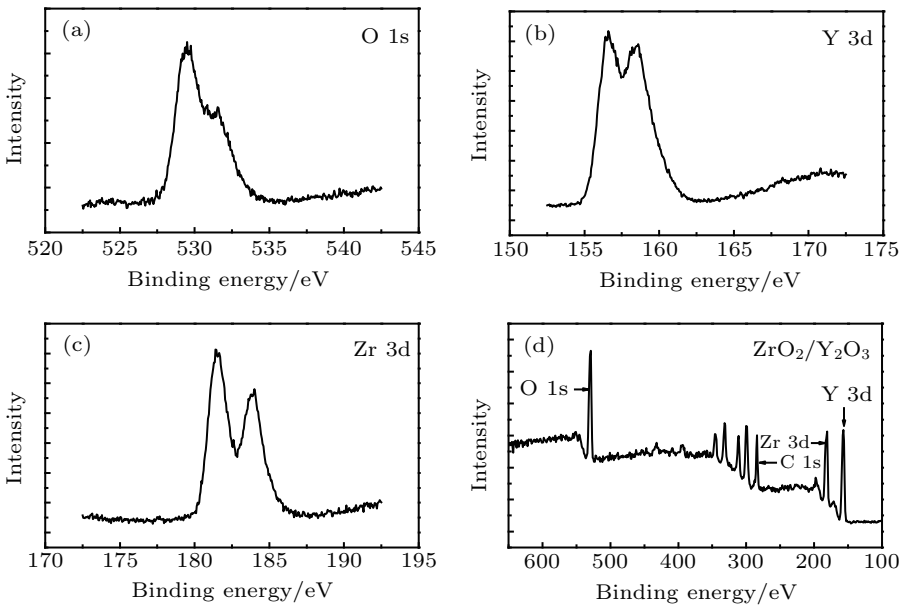


Fig. 1. XPS spectra of the ZrO_2/Y_2O_3: (a) O region; (b) Y region; (c) Zr region; and (d) a survey spectrum.

The peaks centered at 529.48 eV, 156.61 eV, and 181.52 eV correspond to O 1s for the O^{2+} state,[29] Y 3d for the Y^{3+}state, and Zr 3d for the Zr^{4+} state, respectively,[30,31] indicating that the sample is composed of ZrO_2 and Y_2O_3. From the analysis in Table 1, the stoichiometric ratio of the sample is $(ZrO_2)_{0.618}/(Y_2O_3)_{0.382}$.

Table 1. Parameters of Zr 3d, Y 3d, and O 1s in XPS spectra. BE stands for binding energy.

Name	Start BE/eV	Peak BE/eV	End BE/eV	Percentage/at.%
Zr 3d	188.3	181.52	178.25	19.88
Y 3d	163	156.61	153.35	24.62
O 1s	536.5	529.48	525.8	55.5

Figure 2 shows the XRD spectrum for the synthesized $(ZrO_2)_{0.618}/(Y_2O_3)_{0.382}$ sample. All the diffraction peaks can be indexed as the cubic structure in space group $Fm\text{-}\bar{3}m$, and the lattice constant is $a = 5.2044$ Å. The narrow and strong diffraction peaks suggest that the sample is well crystallized.

The impedance spectra of ZrO_2/Y_2O_3 solid solutions under high pressures are shown in Figs. 3(a)–3(d). Although the sample is polycrystalline, only one semicircle can be observed in the spectra, indicating that the grain and grain boundary of the sample have the same response to the alternate-current signal, and therefore they have the same impact on the electrical transport properties; otherwise, two semicircles should be seen. This behavior can be considered as a positive result for practical applications.

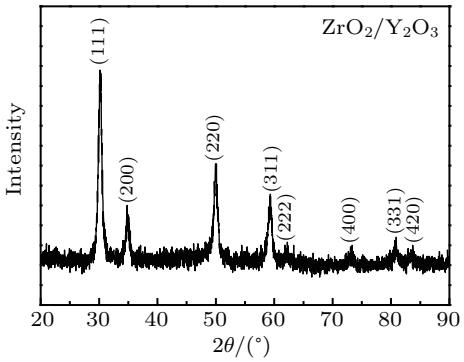


Fig. 2. XRD pattern of the synthesized sample.

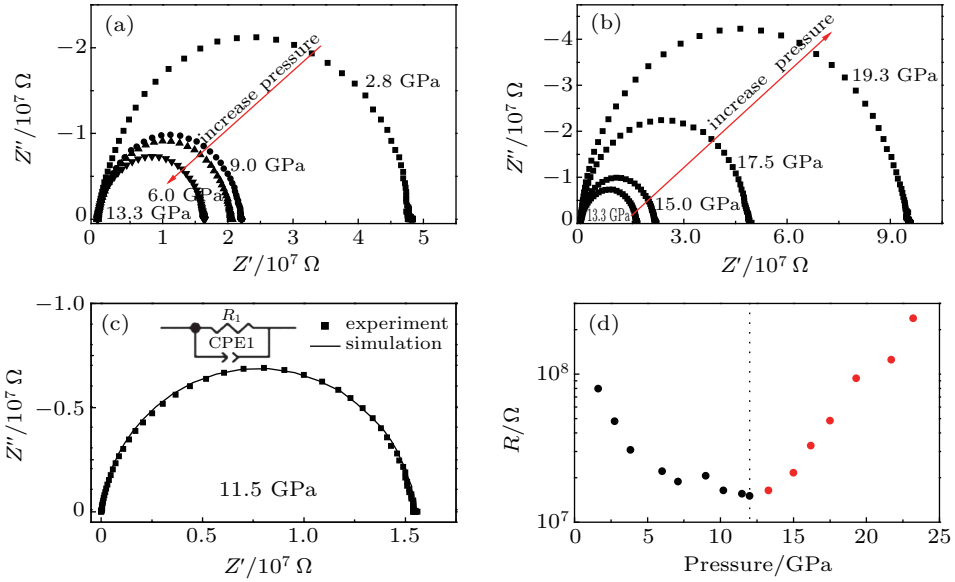


Fig. 3. (a) and (b) Impedance spectra of ZrO_2/Y_2O_3 under high pressures. (c) Fitting result for the impedance spectrum at 11.5 GPa. The fitting error is less than 5%. (d) Pressure dependence of bulk resistance of ZrO_2/Y_2O_3. The black and red lines are guidance for the eyes.

Since the difference between the grain and grain boundary is barely distinguishable, the equivalent circuit model used for further quantitatively analyzing the impedance spectra can be simplified as shown in Fig. 3(c), in which resistor R and constant-phase elements represent the total resistance and capacitance of grains and grain boundaries, respectively. Their parallel arrangement can describe the frequency response to the alternate-current signal. With the equivalent model, the total resistance R can be fitted at different pressures. The pressure dependence of R is shown in Fig. 3(d). It can be found that the pressure-dependent resistance shows two opposite change tendencies. Below 13.3 GPa, the resistance decreases as the pressure increases; but above 13.3 GPa, it increases sharply.

Generally, the most possible reason for the abrupt change in resistance under high pressure is the pressure-induced structural phase transition or metallization.[32,33] However, the pressure-induced metallization should be excluded from our case because the resistance value still remains at a high level ($10^7 - 10^8$ Ω) in the whole experimental pressure region. Thus, the potential pressure-induced structural phase transition in ZrO_2/Y_2O_3 solid solutions is a primary issue that we need to consider in our study, and could be helpful for revealing the mechanism concealed behind the anomalous variation of the electrical transport properties of ZrO_2/Y_2O_3 under high

pressure.

High-pressure XRD measurements are taken for ZrO_2/Y_2O_3 solid solutions up to 25.7 GPa. Selected representative spectra are shown in Fig. 4. It can be seen that all the diffraction peaks shift toward higher 2θ values and exhibit some broadened features due to the evolved nonhydrostatic conditions at high pressures. Except the shifts and broadening, no other obvious changes can be found in the diffraction peaks, suggesting that the crystal symmetry of ZrO_2/Y_2O_3 is stable within the pressure region we have studied. From the patterns of XRD spectra, we cannot see any evidence that the structure phase transition occurs in ZrO_2/Y_2O_3 at high pressures.

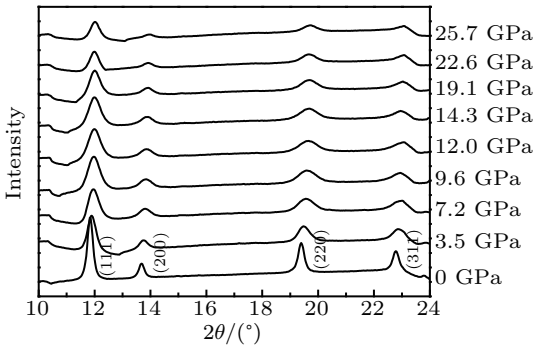


Fig. 4. Representative angle dispersive XRD patterns of ZrO_2/Y_2O_3 at various pressures, with an incident wavelength $\lambda = 0.6199$ Å.

By using the Rietveld fitting method, we analyze the XRD spectra carefully, and obtain the pressure-dependent lattice parameters and the equation of state. Figures 5(a) and 5(b) show the Rietveld refinement results for ZrO_2/Y_2O_3 in the cubic phase ($Fm\text{-}\bar{3}m$) at 9.6 GPa with R_p = 0.23%, wR_p = 0.33%, and at 14.3 GPa with R_p = 0.35%, wR_p = 0.26%, respectively. They fit well with the experimental XRD spectra.

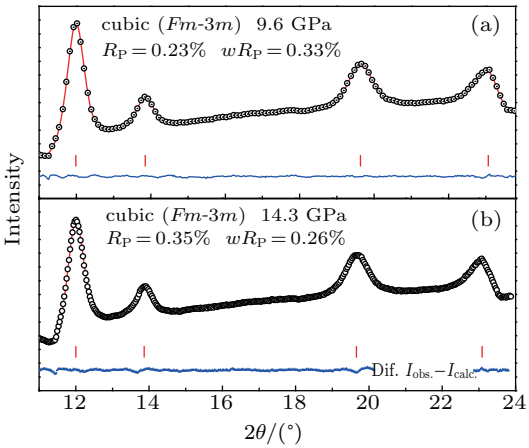


Fig. 5. Representative Rietveld refinement results for XRD spectra of ZrO_2/Y_2O_3 at (a) 9.6 GPa and (b) 14.3 GPa with an incident wavelength $\lambda = 0.6199$ Å.

The pressure-dependent d values of crystal planes (111), (200), (220), and (311) are drawn in Fig. 6. As pressure increases, the d values decrease correspondingly, indicating that the crystal structure becomes more compact. It can be clearly seen that the d values decrease with two different trends before and after 13.1 GPa. The pressure point in Fig. 3(d) happens to be where the total resistance changes abnormally. Pure ZrO_2 has been confirmed to have a pressure-induced phase transition from the monoclinic baddeleyite phase to the orthorhombic phase at approximately 10 GPa, with obvious appearance and disappearance of some diffraction peaks in XRD spectra;[34] however, in our experiment, such behavior is not found. It is suggested that an isostructural phase transition in ZrO_2/Y_2O_3 solid solution should be responsible for the abnormal change in resistance.

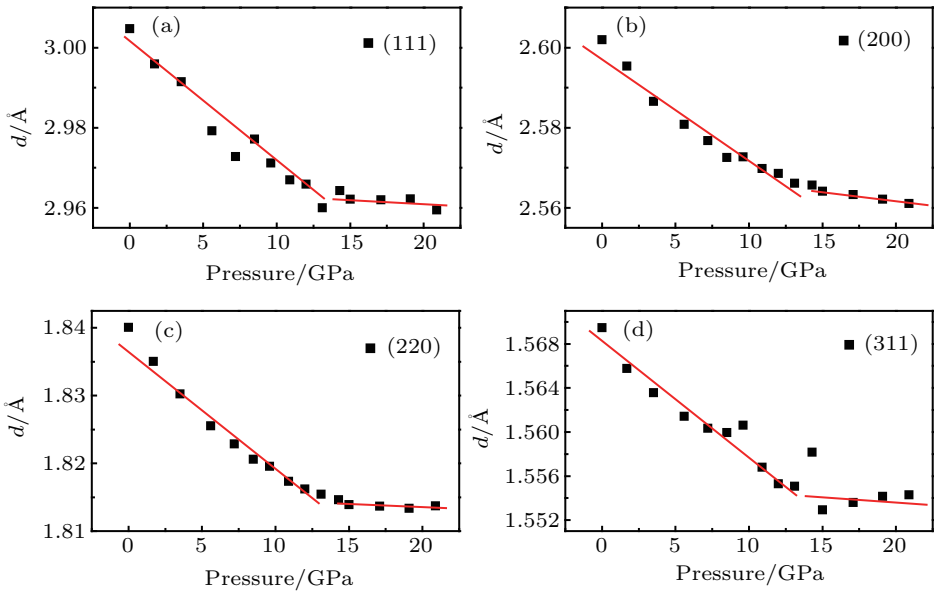


Fig. 6. Pressure dependence of different interplanar spacings: (a) (111), (b) (200), (c) (220), and (d) (311).

The pressure dependence of lattice constants and unit cell volume of ZrO_2/Y_2O_3 can be obtained from the Rietveld fitting results, as shown in Figs. 7(a) and 7(b). It can be seen that the pressure-induced isostructural phase transition is reversible, and no obvious hysteresis is found during decompression. The pressure-dependent unit cell volume is fitted with the Birch–Murnaghan equation of state[35,36]

$$P = \frac{3}{2}B_0\left[\left(\frac{V_0}{V}\right)^{7/3} - \left(\frac{V_0}{V}\right)^{5/3}\right] \times \left\{1 - \frac{3}{4}\left(4 - B_0'\right)\left[\left(\frac{V_0}{V}\right)^{2/3} - 1\right]\right\}, \quad (1)$$

where B_0 and B_0' are the bulk modulus and its pressure derivative at the equilibrium volume, respectively, V_0 and V are the volumes at ambient condition and pressure P, respectively. The fitting results are shown in Figs. 7(c) and 7(d). Below 13.1 GPa, B_0 is determined to be 125.2 GPa at a fixed $B_0' = 4$; meanwhile, above 13.1 GPa, B_0 is 290.3 GPa. The bulk modulus of the ZrO_2/Y_2O_3 solid solution increases by 131.9% at high pressures.

According to the method of least squares,[36] we calculate the standard error values of B_0 in the two pressure stages. The results are shown in Table 2. Although the standard errors are relatively large, the big difference between B_0 values below and above 13.1 GPa is reliable enough to support the conclusion that a pressure-induced isostructural phase transition occurs in the ZrO_2/Y_2O_3 solid solution.

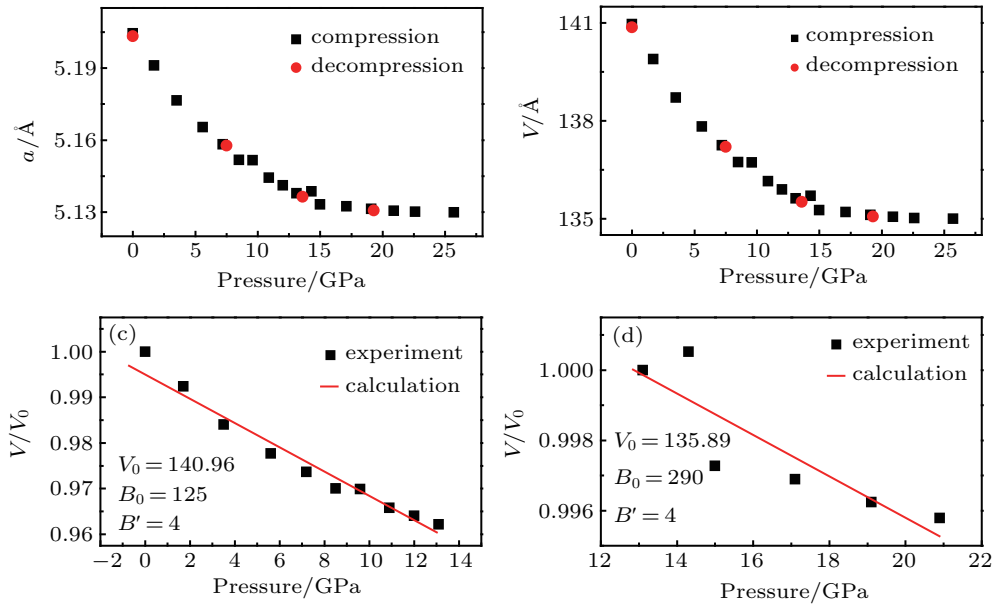


Fig. 7. (a) and (b) Pressure dependence of the lattice constants and the unit cell volume of the cubic ZrO_2/Y_2O_3. (c) and (d) Isothermal compression curves of ZrO_2/Y_2O_3 at ambient temperature in two different pressure stages. The red line is a second-order Birch–Murnaghan fit to the experimental data.

Table 2. B_0 in two different pressure ranges.

Pressure stage/GPa	B_0/GPa	B_0'
below 13.1	125.2(5.6)	4.0 (fixed)
above 13.1	290.3(21.3)	4.0 (fixed)

4. Conclusions

In summary, by combing *in situ* impedance and XRD measurements, we have studied the electrical transport and structural properties of the Y_2O_3-stabilized ZrO_2 solid solution under a high pressure up to 23.2 GPa. The pressure dependence of resistance reveals one potential and unknown change in Y_2O_3/ZrO_2 at 13.3 GPa, which had not been found before. The XRD measurement and Rietveld refinement further confirm that the abnormal change in resistance actually results from the pressure-induced isostructural phase transition in the Y_2O_3/ZrO_2 solid solution. By fitting the volume data with the Birch–Murnaghan equation of state, it is also found that the bulk modulus B_0 of the Y_2O_3/ZrO_2 solid solution increases by 131.9% from 125.2 GPa to 290.3 GPa due to the isostructural phase transition. This study may help deepen our knowledge for future applications of ZrO_2 solid solution-based devices under extreme conditions.

References

[1] Tang Z J, Li R and Yin J 2013 *Chin. Phys. B* **22** 067702
[2] Bell B D C, Murphy S T, Burr P A, Grimes R W and Wenman M R 2015 *J. Appl. Phys.* **117** 084901
[3] Wang J Y, Zhai W, Jin K X and Chen C L 2011 *Chin. Phys. B* **20** 097202
[4] Teterycz H, Klimkiewicz R and Łaniecki M 2003 *Appl. Catal. A Gen.* **249** 313
[5] Calderon-Moreno J M and Yoshimura M 2002 *Solid State Ion.* **154-155** 125
[6] Yamaguchi T 1994 *Catal. Today* **20** 199
[7] Li J, Zhou X M and Li J B 2008 *Rev. Sci. Instrum.* **79** 123107
[8] Dolan D H and Ao T 2008 *Appl. Phys. Lett.* **93** 021908

[9] Yoo C S, Holmes N C, Ross M, Webb D J and Pike C 1993 *Phys. Rev. Lett.* **70** 3931
[10] Borik M A, Bublik V T, Kulebyakin A V, Lomonova E E, Milovich F O, Myzina V A, Osiko V V, Seryakov S V and Tabachkova N Y 2013 *Phys. Solid State* **55** 1690
[11] Chen D J and Mayo M J 1993 *Nanostruct. Mater.* **2** 469
[12] Hahn H 1993 *Nanostruct. Mater.* **2** 251
[13] Mondal P, Klein A, Jaegermann W and Hahn H 1999 *Solid State Ion.* **118** 331
[14] Tuller H L 2000 *Solid State Ion.* **131** 143
[15] Strickler D W and Carlson W G 1965 *J. Am. Ceram. Soc.* **48** 286
[16] Hirano M, Watanabe S, Kato E, Mizutani Y, Kawai M and Nakamura Y 2004 *J. Am. Ceram. Soc.* **82** 2861
[17] Winnubst A J A, Groot Zevert W F M, Theunissen G S A M and Burggraaf A J 1989 *Mater. Sci. Eng. A* **109** 215
[18] Qi Z M, Shi C S, Wei Y G, Wang Z, Liu T, Hu T D, Zhao Z Y and Li F L 2001 *J. Phys.: Condens. Matter* **13** 11503
[19] Zhang L J, Wang Y C, Lv J and Ma Y M 2017 *Nat. Rev. Mater.* **2** 17005
[20] Zhu P W, Tao Q, Wang L, He Z and Cui T 2018 *Chin. Phys. B* **27** 076103
[21] Desgreniers S and Lagarec K 1999 *Phys. Rev. B* **59** 8467
[22] Haines J, Léger J M, Hull S, Petitet J P, Pereira A S, Perottoni C A and da Jornada J A H 2005 *J. Am. Ceram. Soc.* **80** 1910
[23] Yu X H, Li F F, Han Y H, Hong F, Jin C Q, He Z and Zhou Q 2018 *Chin. Phys. B* **27** 070701
[24] He C Y, Gao C X, Ma Y Z, Li M, Hao A M, Huang X W, Liu B B, Zhang D M, Yu C L, Zou G T, Li Y C, Li H, Li X D and Liu J 2007 *Appl. Phys. Lett.* **91** 092124
[25] Han Y H, Gao C X, Ma Y Z, Liu H W, Pan Y W, Luo J F, Li M, He C Y, Huang X W, Zou G T, Li Y C, Li X D and Liu J 2005 *Appl. Phys. Lett.* **86** 064104
[26] Wang Q L, Liu C L, Gao Y, Ma Y Z, Han Y H and Gao C X 2015 *Appl. Phys. Lett.* **106** 132902
[27] Piermarini G J, Block S, Barnett J D and Forman R A 1975 *J. Appl. Phys.* **46** 2774
[28] Yang J M, Gan X S, Zhao Y, Cui M Q, Zhu T, Zhao Y D, Sun L J, Zheng Lei, Yan F, Hu Z M, Wei M X, Zhang J Y and Yi R Q 2011 *Chin. Phys. B* **20** 010705
[29] Huang N K, Colligon J S, Kheyrandish H and Tang Y S 1993 *Nucl. Instr. Meth. B* **80-81** 1101
[30] Majumdar D and Chatterjee D 1991 *J. Appl. Phys.* **70** 988
[31] Ingo G M and Marletta G 1996 *Nucl. Instr. Meth. B* **116** 440
[32] Nayak A P, Bhattacharyya S, Zhu J, Liu J, Wu X, Pandey T, Jin C Q, Singh A K, Akinwande D and Lin J F 2014 *Nat. Commun.* **5** 3731
[33] Matsuoka T and Shimizu K 2009 *Nature* **458** 186
[34] Al-Khatatbeh Y, Lee K K M and Kiefer B 2010 *Phys. Rev. B* **81** 214102
[35] Yang J, Zhu F, Zhang Q, Wu Y, Wu X, Qin S, Dong J C and Chen D L 2013 *Chin. Phys. Lett.* **30** 046101
[36] Fan D W, Wei S Y, Liu J, Li Y C and Xie H S 2011 *Chin. Phys. Lett.* **28** 076101